Original Article

Optimization of Reconstruction Parameters for Discovery 710 Positron Emission Tomography/Computed Tomography

Ahmed Abdel Mohymen, Hamed Ibrahim Farag, Sameh M. Reda[1], Ahmed Soltan Monem[2], Said Abdelfattah Ali[2]

Department of Nuclear Medicine and Radiation Therapy, National Cancer Institute, Cairo University, Cairo, [1]Department of Radiometry, National Institute of Standards, [2]Department of Biophysics, Faculty of Science, Cairo University, Giza, Egypt

Abstract

Aim: This study aimed to optimize the quantitative aspects of (^{18}F) fluorodeoxyglucose (FDG) positron emission tomography (PET)/computed tomography (CT) imaging by investigating the impact of various reconstruction parameters on the recovery coefficients (RCs) using the NEMA image quality phantom. Specifically, the study aims to assess how different matrix sizes, iterations, subsets, and Gaussian postfilters affect the accuracy of standardized uptake value (SUV) quantification in (^{18}F) FDG PET/CT imaging. **Materials and Methods:** The study utilized the "Vue Point FX + Sharp IR" algorithm for PET image reconstruction, incorporating 3D-ordered subset expectation maximization (3D-OSEM), time-of-flight, and point spread function technologies. Various reconstruction parameters were explored, including two distinct matrix sizes, multiple iterations, subsets, and a wide range of Gaussian postfilters. The investigation focused on the impact of these parameters on RCs using the NEMA image quality phantom. **Results:** The results of the study indicated that for accurate SUV quantification in spheres ≥17 mm, the 256 × 256 matrix size and mean SUV should be employed. Conversely, for spheres ≤13 mm, maximum SUV was found to be more suitable. The choice of postfiltering value was shown to have a significant impact on SUV quantification accuracy, particularly for small-sized spheres. In addition, a larger matrix size was found to partially mitigate the effects of Gibbs artifact and slightly enhance SUV quantification for the spheres of various sizes. **Conclusion:** This study highlights the critical importance of optimizing PET reconstruction parameters in accordance with the guidelines set by European Association of Nuclear Medicine/EARL. By optimizing these parameters, the accuracy and reliability of SUV quantification in (^{18}F) FDG PET imaging can be significantly enhanced, especially for small-sized spheres. This underscores the necessity of carefully considering reconstruction parameters to ensure precise and reliable quantitative measurements in PET/CT imaging.

Keywords: (^{18}F) fluorodeoxyglucose positron emission tomography/computed tomography optimization, European association of nuclear medicine/EARL guidelines, gaussian filters, gibbs artifacts, standardized uptake value, time-of-flight-point spread function-based reconstruction, voxel sizes

Received on: 03-10-2024 **Review completed on:** 02-12-2024 **Accepted on:** 06-12-2024 **Published on:** 24-02-2025

Introduction

Positron emission tomography/computed tomography (PET/CT) system is an essential diagnostic tool in oncology that serves various purposes including diagnosis, staging, restaging, prognosis, and therapeutic monitoring. In clinical practice, standardized uptake value (SUV) is widely employed in clinical practice as a diagnostic and prognostic metric.[1,2] However, there are various factors causing measurement errors in clinical practice, as discussed extensively in.[3-5] These factors can be divided into two categories: biologic factors and physical/technological factors. PET systems in hospitals vary in technology with a variety of systems installed. Even within the hybrid PET/CT period, some scanners have been in use for more than 15 years, while others incorporate the latest state-of-the-art hardware and software technologies. In addition, hospitals may adopt different acquisitions and reconstruction parameters to maximize lesions detectability based on their scanner's technological capabilities.[3,6,7] The evolution of technologies enhanced the diagnostic capabilities

Access this article online

Quick Response Code:

Website: www.jmp.org.in

DOI: 10.4103/jmp.jmp_167_24

Address for correspondence: Dr. Said Abdelfattah Ali, Department of Biophysics, Faculty of Science, Cairo University, Giza, Egypt. E-mail: saidataha@cu.edu.eg

How to cite this article: Mohymen AA, Farag HI, Reda SM, Monem AS, Ali SA. Optimization of reconstruction parameters for discovery 710 positron emission tomography/computed tomography. J Med Phys 2025;50:118-30.

of PET scanners. Nonetheless, the variety of available technologies, both in terms of hardware and software, has resulted in variations in image quality and SUV quantifications which are dependent on the scanner technologies and methods of reconstruction used.[2,8,9] The limited spatial resolution of PET scanners affects the quantification of small size lesions caused by partial volume effect (PVE). This effect interrupts SUV quantification, specifically in lesions sizes that are smaller than three times the spatial resolution of PET scanner.[10] PVE can be minimized by implementing time-of-flight (TOF) data and point spread function (PSF) correction for resolution recovery in newer PET/CT scanners.[11] These approaches are possible due to the development of fast scintillators such as lutetium oxyorthosilicate and lutetium-yttrium oxyorthosilicate, which allow for the measurement of TOF-the difference in the time of arrival of the two annihilation photons.[12] The TOF data are converted into a Gaussian distribution of the probability of the annihilation position along the line of response, which improves the signal-to-noise ratio (SNR) in PET images.[12-16] Although the PSF corrections improve the resolution and uniformity of PET images, it can result in an upward bias of the maximum SUV (SUVmax). This is due to the higher variance at the voxel level which causes over-enhancement of sharp transitions at lesion margins, resulting in edges enhancement known as the Gibbs artefact.[17,18] The heterogeneity in PET quantification metrics, particularly SUVmax and mean SUV (SUVmean), is extremely important, especially in clinical trials or multicenter studies that utilize these metrics.[7] To optimize the performance of the PET/CT system which involves achieving better image quality and more accurate SUV quantification, it is necessary to fine-tune the reconstruction parameters.[19] In 2018 the European Association of Nuclear Medicine (EANM) recommended a SUV harmonization approach that involves reconstructing two datasets: an European Association Research Ltd (EARL)-approved reconstruction setting that meets standardized performance specifications for quantitative assessment, and an additional reconstruction optimized for optimal visual assessment to maximize lesion detectability for qualitative interpretation.[1,20] To ensure the accuracy of quantitative evaluations, SUV recoveries obtained from the first dataset must remain within the recovery coefficient (RC) bandwidths established by EARL. As modern PET/CT system progress, it has been proposed to update the EANM/EARL recommendations to reflect these advancements.[21] Scanner optimization ensures maximum accuracy in quantitative imaging for individual PET/CT systems, while harmonization focuses on reproducibility across scanners, enabling consistent comparisons essential for multi-center studies. Balancing these ensures both high performance and reliable, standardized results.

The objective of this study was to find the optimal reconstruction parameters for the Discovery 710 PET/CT system to identify reconstruction parameters that optimize precise SUV determination without compromising image quality while using the combined TOF + PSF algorithm. The study's purpose is to optimize the number of iterations, subsets, postfilterings, and matrix sizes, as these variables have a significant impact on the qualitative and quantitative aspects of (^{18}F) fluorodeoxyglucose (FDG) PET imaging.

Materials and Methods

The phantoms utilized, along with the filling procedures employed, were consistent with the image quality quality control (QC) measurement guidelines established by EANM/EARL.[1,20]

Phantoms

Jaszczak flood phantom

In the current work, a cross-calibration factor was investigated to assess the concordance of activity concentrations (kBq/ml) between the estimated activity concentrations values derived from PET images using a PET scanner and the predicted values measured by a dose calibrator. A solution of (^{18}F) FDG (37 MBq, as measured by the dose calibrator) was added to a flood phantom with interior dimensions of 8.5 "diameter × 7.32" height (21.6 cm × 18.6 cm) and a precisely known volume of 6.9 L. The phantom was then filled with water, yielding a solution with exactly defined activity concentration. A two-bed acquisition of the phantom was performed, and the raw data of PET-phantom images were reconstructed using attenuation and scatter correction settings identical to those employed in patient studies.

Upon completion of the images reconstruction, the SUVmean (kBq/ml) was determined by defining a region of interest (ROI) on one transverse slice with a diameter at least 3 cm smaller than the diameter of the uniform cylindrical phantom and then copying that ROI, to all consecutive transverse slices (except the first and last slice). The average of mean SUVs for all ROI's throughout the phantom was calculated as measured by the PET scanner. To calculate the cross-calibration factor, the average activity concentration of the phantom PET images measured with the PET scanner was divided by the activity concentration measured with the dose calibrator at the start of the phantom filling. The cross-calibration factor was found to be 0.91, which is aligned with.[22] Furthermore, the clocks of the PET acquisition workstation and the dose calibrator were synchronized.

NEMA body phantom

The NEMA body phantom had a background compartment with a volume of 9.7 L and equipped with six fillable spheres had different inner size diameters ranging from 10, 13, 17, 22, 28, and 37 mm. At the start of the measurements, the background compartment and spherical inserts were filled with (^{18}F) FDG solutions containing 2.0 and 20 kBq/mL of activity, respectively. As a result, the sphere-to-background ratio was 10-1. The current study utilized phantom imaging procedures by positioning the phantom on the PET/CT table and aligning it using a CT laser marker in accordance with the NEMA NU 2–2007 guidelines.

Positron emission tomography/computed tomography scanners

For the imaging procedures, a PET/CT Discovery 710–GE Healthcare (Milwaukee, WI, USA) was used, in accordance with the current EANM/EARL guidelines for (^{18}F) FDG image quality QC phantom imaging.[23,24] The data acquisition and images reconstruction were performed using the software implemented in the Discovery 710 PET/CT Advantage Workstation Volume Share 5 (AW 4.6) release. The technical specifications of the PET/CT Discovery 710 system are found in Table 1.[25]

Acquisitions and reconstruction parameters

To analyze NEMA phantom, a routine quantitative whole-body PET/CT scans were performed in a two bed position for 10 min, which including a low-dose CT scan for attenuation correction and localization purposes**.** To determine the optimal reconstruction parameters for image quality enhancement, the study investigated various numbers of iterations, subsets, Gaussian filters, and pixel sizes. Prior studies revealed that two or three iterations were sufficient to compromise and achieve optimal SNR.[26] A fully 3D Maximum-Likelihood Ordered Subset Expectation Maximization (3D ML-OSEM) algorithm was utilized for images reconstruction with all corrections applied. The images were reconstructed using the (Vue Point FX + Sharp IR) 3D-OSEM + TOF + PSF. The two matrices sizes had the following specifications: a diagonal size of 39, pixel sizes of 2.73, and 3.64 mm and voxel sizes of 6.1 and 8.1 mm^3, respectively. In addition, postreconstruction filters with full width at half maximum (FWHM) ranging from 4 mm to 10 mm, in increments of 0.5 mm, were used, as detailed in Table 2.

Table 1: Technical characteristics of discovery 710 positron emission tomography/computed tomography scanner

PET detector	Specifications
Gantry dimensions (cm)	192×226.1×140
Weight (kg)	4916
Patient port (cm)	70
Scintillator material	LYSO
Scintillator dimensions (mm)	4.2×6.3×25
Crystal array per block	9×6
Number of detector rings	24
Number of crystals per ring	576
Number of crystals	13,824
Number of PMTs	1024 (256 quad-anode)
Number of image planes	47
Vertical travel (cm)	2.5–20.5 below the isocenter
Acquisition modes	3D, 4D
Coincidence window (ns)	4.9
Lower energy threshold (keV)	425
Maximum axial coverage (cm)	170–200
Axial field of view (cm)	15.7
Trans-axial field of view (cm)	70
Slice overlap	User defined 1–23, minimum recommendation 5 (10% overlap)
Image matrix sizes	128×128, 192×192, 256×256
Transmission source	CT attenuation correction

LYSO: Lutetium-yttrium oxyorthosilicate, PET: Positron emission tomography, 3D: Three-dimensional, 4D: Four-dimensional, CT: Computed tomography, PMTs:Photo-multiplier tubes

Data analysis

In this work, the analysis of PET/CT reconstructed images was performed using a GE Healthcare Advantage Workstation. The software's processing tools were employed to delineate the percentage of volume of interest at 50% (VOI 50%) on PET images for each sphere, using the predefined XY plane. To ensure consistency, the reconstructed PET slice with the largest diameter among all spheres was selected to adjust the VOI 50% measurements. Following the image quality assessment guidelines outlined by NEMA NU 2-2007, the SUVmax and SUVmean were determined for all spherical inserts. The SUVs values for the six spherical inserts were determined based on the 50% background-corrected isocontour VOI (SUVmean) and the maximum voxel value included in the VOI (SUVmax). For the $SUV_{background}$, for each sphere, a six ROIs of fixed dimensions (diameters equal to the physical inner diameter of the spheres) were defined. They were placed in regions that did not contain any hot sphere, and they were not allowed to intersect. Taking the mean SUV of 6 ROIs for each sphere resulted in the $SUV_{background}$ used for RC calculation. SUVmean incorporates information from multiple voxels, making it less sensitive to image noise. However, it is subject to intra-and inter-observer variability. On the other hand, SUVmax represents the highest voxel value within the VOI and is independent of VOI definition; nonetheless, it is more susceptible to noise.[4]

Quantitative analysis

The RC was used as a quantitation method to investigate the effect of the investigated reconstruction parameters on SUVs measurements of hot spherical inserts in reconstructed images. The RC is defined as follows:[23]

$$RC = \frac{SUV\ Measured\ in\ sphere - Measured\ SUV\ background}{SUV\ Calculated\ in\ sphere - Calculated\ SUV\ background}$$

where

($SUV_{measured}$, measured [max and mean] activity concentration in (kBq/ml) obtained from the reconstructed PET images of phantom).

($SUV_{calculated}$, true activity concentration in [kBq/ml] determined by dose calibrator during filling of spherical inserts).

$Measured\ SUV_{background,}$ mean activity concentration in (kBq/ml) measured from the reconstructed PET images of background compartment of NEMA phantom.

$Calculated\ SUV_{background,}$ mean activity concentration in (kBq/ml) measured from the dose calibrator during filling of phantom background.

Table 2: The reconstruction parameters for phantom-analyzed images

Groups	Recon parameters					
	Iteration number	Subset number	Matrix size	Algorithm	Z-axis filter	Postfiltering range (mm)
Group 1	2	18	192×192	OSEM+PSF+TOF	Standard	4:10
	2	18	256×256	OSEM+PSF+TOF	Standard	4:10
Group 2	2	24	192×192	OSEM+PSF+TOF	Standard	4:10
	2	24	256×256	OSEM+PSF+TOF	Standard	4:10
Group 3	3	18	192×192	OSEM+PSF+TOF	Standard	4:10
	3	18	256×256	OSEM+PSF+TOF	Standard	4:10
Group 4	3	24	192×192	OSEM+PSF+TOF	Standard	4:10
	3	24	256×256	OSEM+PSF+TOF	Standard	4:10

OSEM: Ordered subset expectation maximization, PSF: Point spread function, TOF: Time-of-flight

The RCs reference bandwidths specified by EANM/EARL for RCmean and RCmax as a function of different sphere sizes (mm) were the main standard ranges used to evaluate the RCs plots.[20,27] To evaluate the RCs performance of the investigated reconstruction parameters, they were compared to the recommended RCs specifications provided by EARL2, as shown in Table 3.

Visual analysis

In addition to the quantitative analysis, visual analysis of the RCs curves was used to identify any abnormal behavior, such as Gibbs artifacts. The optimal reconstruction parameters were selected based on their RCmean and RCmax performance.

Selection of optimizing reconstruction parameters

The RCmean and RCmax of the reconstructed phantom images were plotted versus spheres sizes. The optimum reconstruction parameters were selected based on the analysis of the quantitative characteristics and the visual appearance of the RCs curves at various reconstruction parameters. Furthermore, the bandwidth of RCs should be consistent with the current EARL specification limits, and optimizing RCs curves should not demonstrate significant overshoots (upward bias) due to Gibbs artifacts.[20,23]

Results

According to the specifications established by EARL/EANM,[28] this study aimed to assess the impact of iterations, subsets, postfilterings, and matrix sizes on the RCs of various sphere sizes as follows:

Quantitative analysis

The Discovery 710 PET/CT system was optimized by investigating four different reconstruction parameters groups, as shown in Table 2. Figures 1-16 shows the RCs curves, demonstrating the correlation between RCmax, RCmean, and various sphere sizes.

During this investigation, it was found that various combinations of the investigated reconstruction pentameters had almost identical effects on RCmax. This effects resulted in fewer distinct behaviors on certain RCmax curves. The following details provide a comprehensive overview for these findings:

Table 3: The recommended standardized uptake value recovery coefficients for ^{18}F based on the EARL 2 recovery coefficient max/mean recovery coefficient specifications[28]

IEC phantom spheres		^{18}F standards 2 RCs	
Diameter (mm)	Volume (mL)	Maximum	Mean
37	26.52	1.05–1.29	0.85–1.00
28	11.49	1.01–1.26	0.82–0.97
22	5.57	1.01–1.32	0.80–0.99
17	2.57	1.00–1.38	0.76–0.97
13	1.15	0.85–1.22	0.63–0.86
10	0.52	0.52–0.88	0.39–0.61

RCs: Recovery coefficients, IEC: International Electro-technical Commission

First, when 2 iterations, 18 subsets, and a matrix size of 192 × 192 were utilized, postfilterings 6.4, 6.5, and 7 mm produced similar RCmax values.

Second, for 2 iterations, 24 subsets, and a matrix size of 192 × 192, postfilterings 5.5 and 6 mm produced comparable RCmax values.

Moving on to 3 iterations, 18 subsets, and a matrix size of 192 × 192, postfilterings 6 and 6.5 mm exhibited similar RCmax values.

Finally, with 3 iterations, 24 subsets, and a 192 × 192 matrix size, postfilterings 6, 7, and 8 mm had similar RCmax values.

These findings shed light on the relationship between iterations, subsets, postfilterings, matrix sizes, as well as their influences on RCmax.

Postfiltering effect

The effect of postfiltering on the RCs of spheres with various sizes was found to be significant. The present work showed that at postfiltering 4 mm, there was an overestimation/overshooting in the RCs values for sphere sizes of 13, 17, and 22 mm, as shown in Figure 17. In ideal status, as the spheres size decreased, its RCs values decreased consistently. However, the deviation from ideal status was observed at postfiltering 4 mm due to the presence of the overshooting. This overshooting resulted in unexpected fluctuations in the

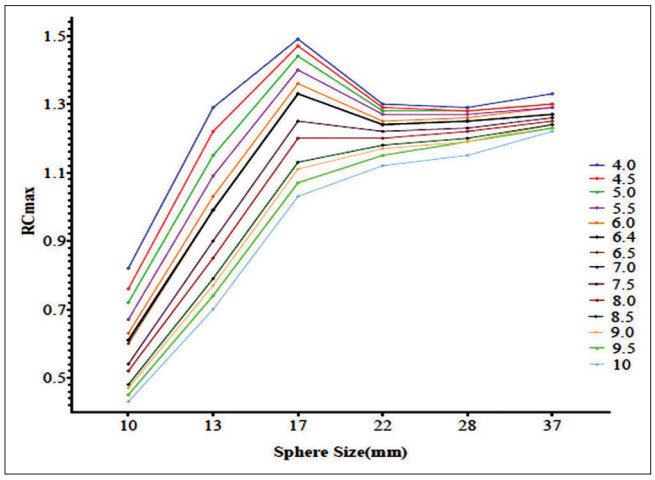

Figure 1: The relation between RCmax and different sphere sizes for 2 iterations, 18 subsets and 192 × 192 matrix size at a wide range of postfiltering values (mm)

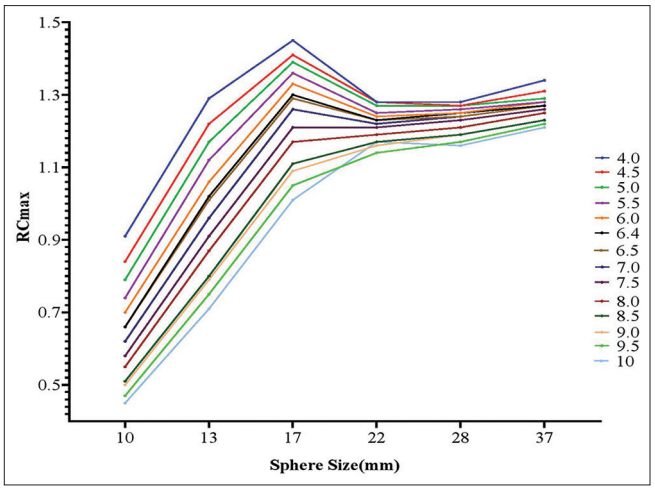

Figure 2: The relation between RCmax and different sphere sizes for 2 iterations, 18 subsets and 256 × 256 matrix size at a wide range of postfiltering values (mm)

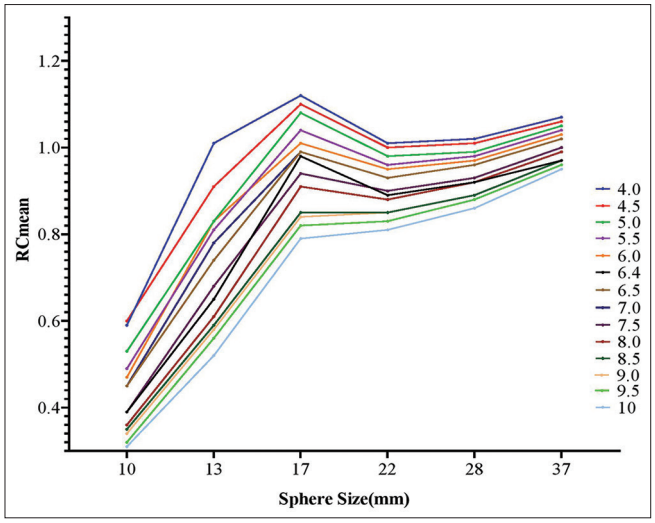

Figure 3: The relation between RCmean different sphere sizes for 2 iterations, 18 subsets and 192 × 192 matrix size at a wide range of postfiltering values (mm)

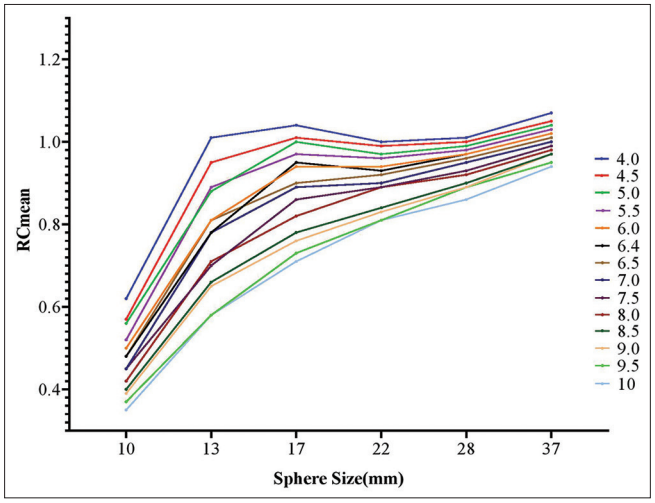

Figure 4: The relation between RCmean different sphere sizes for 2 iterations, 18 subsets and 256 × 256 matrix size at a wide range of postfiltering values (mm)

RCs values rather than a consistent decrease with decreasing the spheres sizes. The overestimation and/or overshooting phenomenon mainly occurred in the RCs of large spheres due to the presence of Gibbs artifacts. Furthermore, these artifacts affected the RCs of small spheres, but they compensated for the loss in the RCs values that caused by the PVE. Compared to RCmean, the overestimations/overshootings had a more pronounced effect on RCmax. Furthermore, higher postfiltering values increased the degree of PVE and caused blurring in small-sized spheres due to the limited spatial resolution of PET scanner, as illustrated in Figure 18. High postfiltering values mitigated the overestimation and overshooting in RCs of large spheres. This meant that higher postfiltering values resulted in a better RCs quantification for large spheres. However, for small-sized spheres, further increasing in postfiltering values resulted in a decrease in their RCs, as depicted in Figure 17, at postfiltering 10 mm. The size of the postfilter had a greater effect on the image quality and RCs quantification of various spheres sizes, as demonstrated in Figure 18. High postfiltering resulted in stronger smoothing but increased image blurring. In contrast, small postfiltering values allowed the filter to consider fewer voxels in the image, resulted in less image blurring compared to large postfiltering. In the present study, the optimal filter size was found to be around 4–4.5 mm and 6–6.5 mm for SUVmean and SUVmax, respectively. Furthermore, two sets of reconstructed images should be used during PET images interpretations, one for image detectability and the other for image quantification, as the overshooting effect and blurring were evident when inadequate filtering was applied to the reconstructed images.

Matrix size effect

When comparing a 256 × 256 matrix size to a 192 × 192 matrix size, it was found that larger matrix size had a minimal

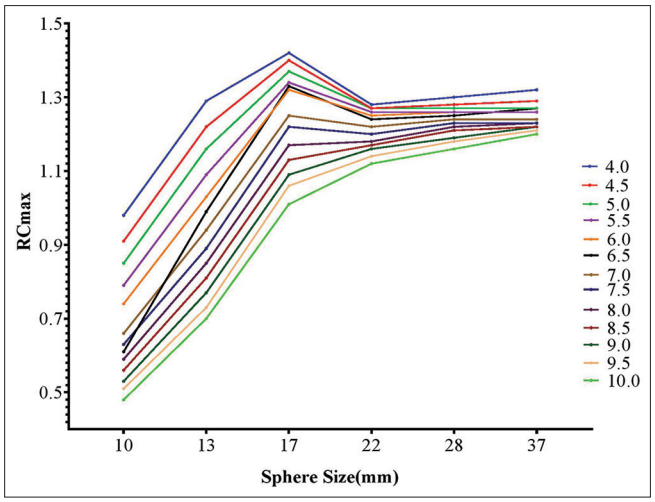

Figure 5: The relation between RCmax and different sphere sizes for 3 iterations, 18 subsets and 192 × 192 matrix size at a wide range of postfiltering values (mm)

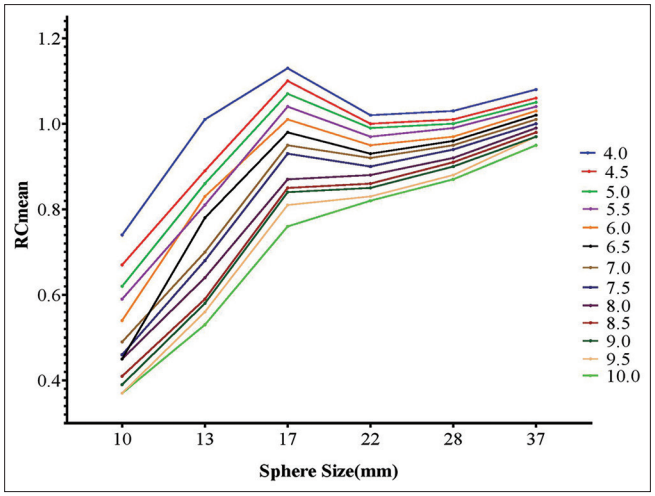

Figure 7: The relation between RCmean and different sphere sizes for 3 iterations, 18 subsets 192 × 192 matrix size at a wide range of postfiltering values (mm)

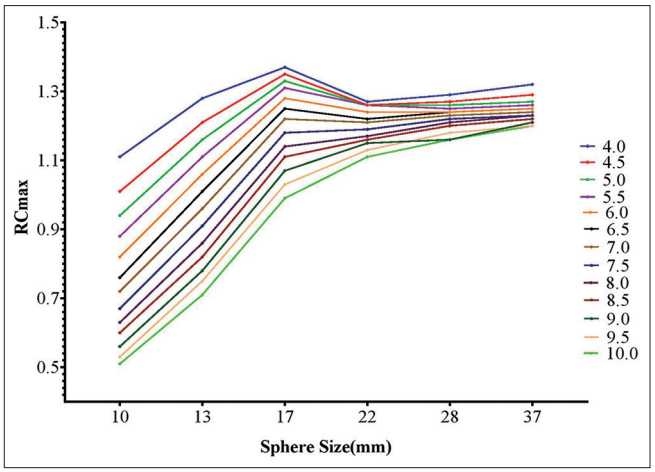

Figure 6: The relation between RCmax and different sphere sizes for 3 iterations, 18 subsets 256 × 256 matrix size at a wide range of postfiltering values (mm)

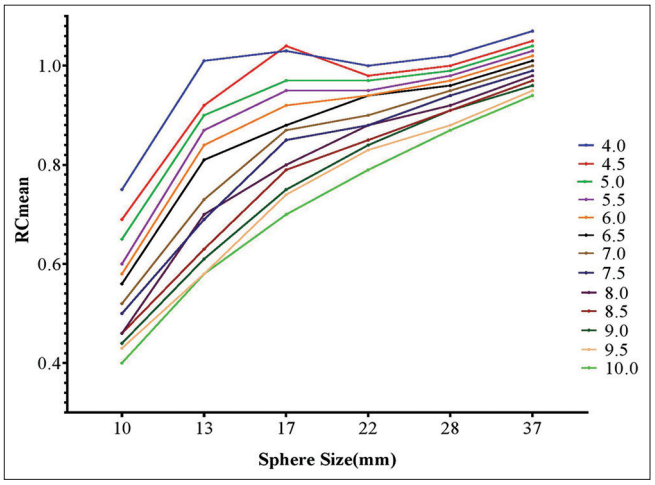

Figure 8: The relation between RCmean and different sphere sizes for 3 iterations, 18 subsets 256 × 256 matrix size at a wide range of postfiltering values (mm)

effect on reducing overestimation in RCs caused by the overshooting effect for large sphere sizes. Furthermore, it slightly decreased the underestimation caused by PVE in small-sized spheres, as depicted in Figure 19. Larger matrix size reduced the negative patterns caused by the overshooting effect, resulted in more accurate measurements of RCs for larger spheres. In addition, increasing the matrix size reduced the impact of PVE, resulted in decreasing underestimation in RCs of small-sized spheres. When comparing the effects of postfiltering and matrix size, it was found that postfiltering had a more significant effect on the RCs quantification than matrix size, as shown in Figures 17 and 19. When utilizing a larger matrix, especially in combination with inadequate postfiltering, it resulted in increased image blurring, as shown in Figure 18. In conclusion, increasing the matrix size had a slight but significant effect on reducing the RCs overestimation caused by Gibbs artifacts in large spheres sizes while decreasing the underestimation produced by PVE in small-sized spheres. However, the effect of postfiltering surpassed the effect of matrix size and had a more significant role in improving the RCs quantification. The 256 × 256 matrix size played a crucial role in minimizing the impact of the overshooting effect and PVE across various spheres sizes, especially when utilizing appropriate postfiltering value.

Iterations and subsets effect

In the present work, optimizing the number of iterations and subsets resulted in a more accurate quantification of RCs values. This effect was particularly beneficial for small-sized spheres, where accurate quantification is challenging due to the PVE. As shown in Figures 20 and 21, increasing the iteration numbers from 2 to 3 had a positive effect on the RCs of small-sized spheres 10 and 13 mm affected by PVE. Furthermore, it decreased the impact of the overshooting at

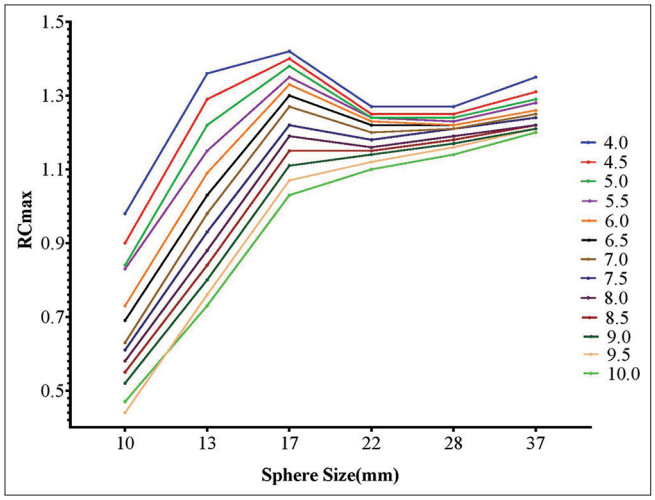

Figure 9: The relation between RCmax and different sphere sizes for 2 iterations, 24 subsets 192 × 192 matrix size at a wide range of postfiltering values (mm)

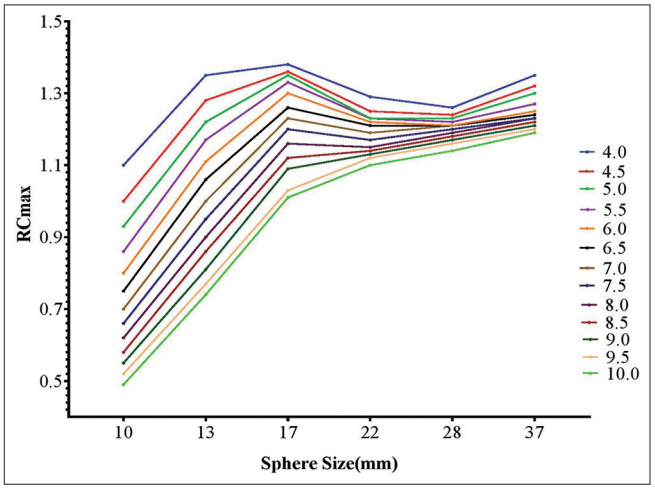

Figure 10: The relation between RCmax and different sphere sizes for 2 iterations, 24 subsets 256 × 256 matrix size at a wide range of postfiltering values (mm)

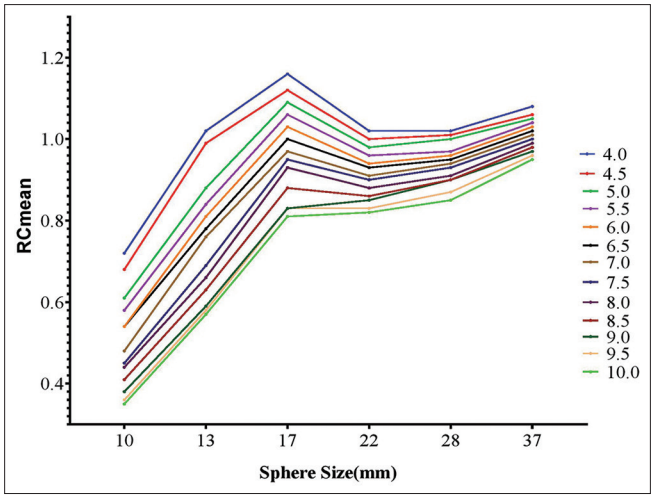

Figure 11: The relation between RCmean and different sphere sizes for 2 iterations, 24 subsets 192 × 192 matrix size at a wide range of postfiltering values (mm)

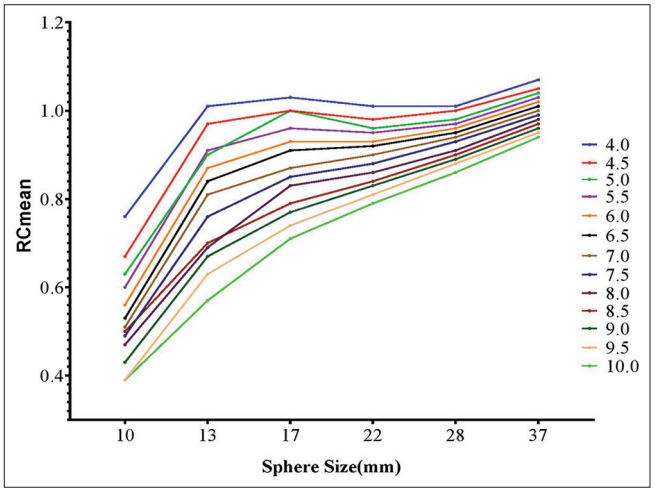

Figure 12: The relation between RCmean and different sphere sizes for 2 iterations, 24 subsets 256 × 256 matrix size at a wide range of postfiltering values (mm)

17 and 22 mm spheres. Furthermore, increasing the number of subsets allowed for a more comprehensive sampling of the data, resulted in enhancing the RCs quantification, particularly for small-sized spheres 10, 13, and 17 mm. In this study, the overshooting effect increased the RCs for spheres with diameters of 13 and 10 mm as the number of iterations increased. The magnitude of the overshooting effect depended on the sphere sizes, matrix sizes, number of iterations, number of subsets, and postfiltering value. The underestimation of RCs at small spheres was related to the PVE, which increased as sphere size decreased. PVE decreased with decreasing the number of iterations. Figures 20 and 21 show how the number of iterations and subsets affects the RCs of various sphere sizes. Optimizing the numbers of subsets and iterations is important for increasing the efficiency of computation time and achieving better RCs quantification. It is preferable to reduce the reconstruction time by decreasing the number of iterations and increasing the number of subsets while keeping optimal RCs. In conclusion, the number of iterations and subsets had a substantial effect on RCs quantification, particularly for small-sized spheres. The present work suggested that combining 3 iterations and 24 subsets was a superior alternative for optimizing the reconstruction process, which resulted in improving the RCs quantification of small-sized spheres, particularly 10 mm sphere.

Visual analysis

Figures 1-16 show the visual analysis of the RCs curves, which assisted in identifying the abnormal behavior or localized alterations of the investigated reconstruction parameters, including Gibbs artifacts. The harmonized reconstruction parameters were selected by simultaneous analyzing the quantitative characteristics of the reconstruction parameters

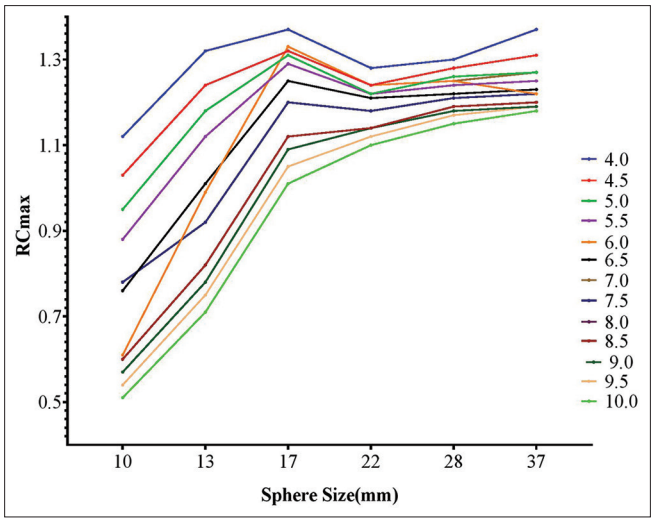

Figure 13: The relation between RCmax and different sphere sizes for 3 iterations, 24 subsets 192 × 192 matrix size at a wide range of postfiltering values (mm)

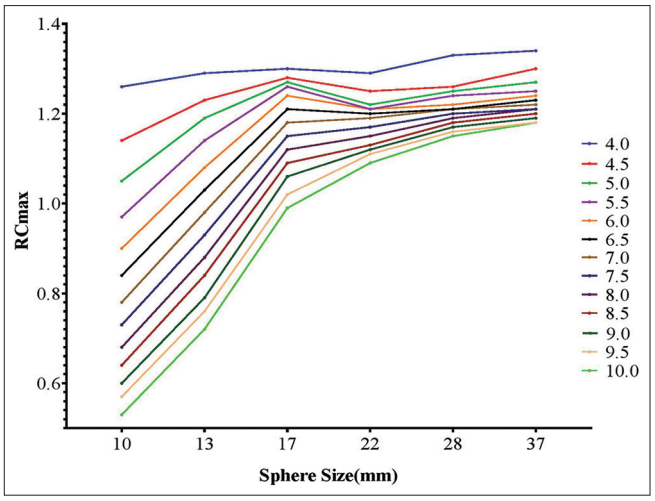

Figure 14: The relation between RCmax and different sphere sizes for 3 iterations, 24 subsets 256 × 256 matrix size at a wide range of postfiltering values (mm)

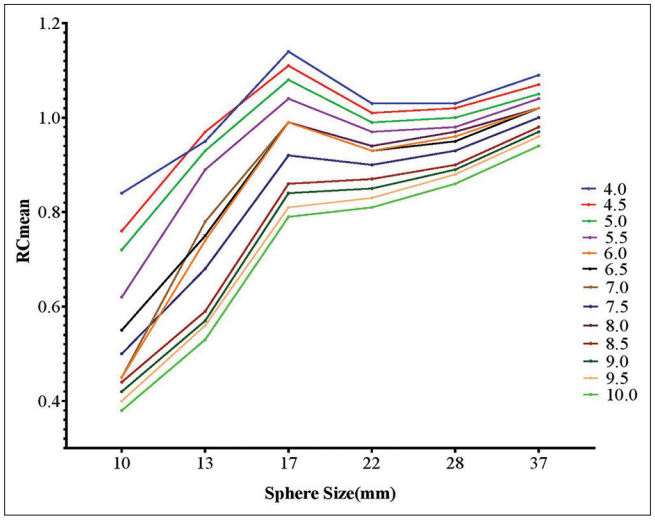

Figure 15: The relation between RCmean and different sphere sizes for 3 iterations, 24 subsets 192 × 192 matrix size at a wide range of postfiltering values (mm)

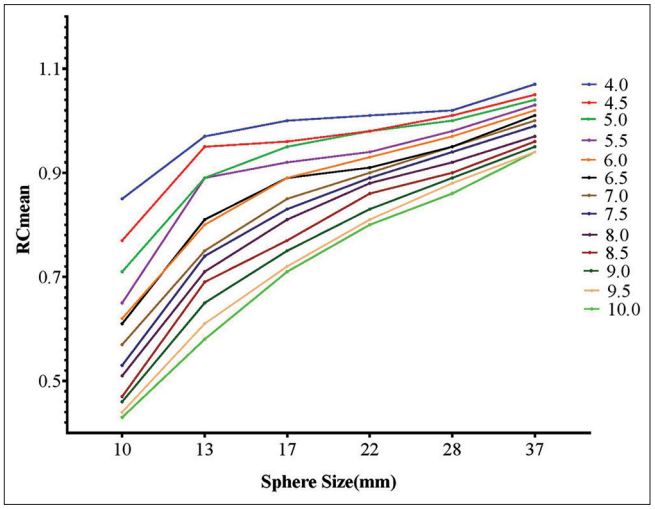

Figure 16: The relation between RCmean and different sphere sizes for 3 iterations, 24 subsets 256 × 256 matrix size at a wide range of postfiltering values (mm)

and the visual appearance of the RCs curves. The selection of reconstruction parameters for harmonization was based on the performance of RCmean and RCmax. The optimal choice of PSF + TOF reconstruction parameters will involve a trade-off between sphere detectability and avoiding Gibbs artifacts that influence RCs quantification. Visual analysis of the RCs curves, Figures 1-16, assisted to identify optimal RC curve that was consistent with the predefined RC specifications by EARL 2. In this work, the RCmax of spheres sizes ≥13 mm exceeded unity due to the influence of Gibbs artifacts, as SUVmax was highly sensitive to these artifacts. In contrast, RCmean was close to or less than unity, whereas SUVmean was less affected by Gibbs artifacts. Furthermore, the presence of Gibbs artifacts caused a nonmonotonic decreasing in RCs values for sphere sizes of 13, 17, and 22 mm. However, when utilizing a matrix size of 256 × 256 and SUVmean, the effect of Gibbs artifacts on spheres measuring 13, 17, and 22 mm was decreased.

When considering the various reconstruction parameters for harmonization, it was observed that the larger spheres showed a significant increase in recoveries. As a result, the resulting RC curves have become more "flat," reducing the dependence of subsequent quantitative analysis on sphere size. The reconstruction parameters in Table 4 show that recoveries for spheres with a diameter of ≥17 mm are essentially independent of size. When utilizing SUVmax for PET/CT quantification, a positive bias of 10%–25% in RC values is acceptable for larger homogenous spheres ≥17 mm.

Finally, the present work proposed that a large matrix size should be utilized with SUVmean to quantify spheres sizes ≥13 mm,

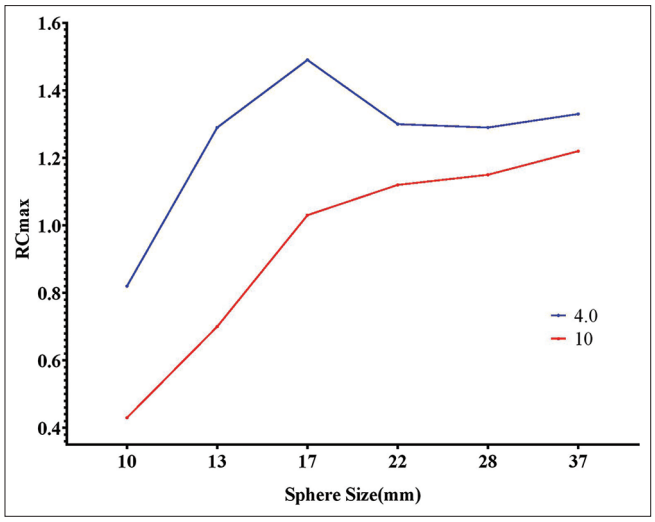

Figure 17: The effect of two different postfiltering values on RCmax at 2 iterations, 18 subsets, and 192 × 192 matrix sizes

while utilizing SUVmax for spheres sizes ≤10 mm. The optimal reconstruction parameters were identified, which resulted in improving SUVmax quantification when utilizing the combined TOF + PSF reconstruction algorithms in this work, as presented in Table 4 and Figure 22.

This study highlights the importance of selecting appropriate reconstruction parameters for better SUVmax/SUVmean quantification in PET/CT. SUVmax was more suitable for quantifying sphere sizes ≤10 mm, while SUVmean was more suitable for sphere sizes ≥13 mm.

Finally, the optimal postfiltering range for SUVmax was 6–6.5 mm, whereas the most suitable postfiltering range for SUVmean was 4–4.5 mm. Table 5 presents the obtained RCs values produced using the optimal reconstruction parameters proposed by this study, which include 3 iterations, 24 subsets, a postfilter value 6.5 mm, and a matrix size 256 × 256. These RC values aligned with the recommended RCs proposed by EARL 2.

Tables 6 and 7 present the optimal reconstruction parameters specifically selected for the routinely used matrix size. These parameters were determined to achieve the best performance when utilizing both SUVmax and SUVmean in the investigated groups. This approach ensures that the drawbacks[29] of larger matrix sizes are mitigated while maintaining reliable and accurate quantitative PET CT imaging.

Table 4: The optimal selected reconstruction parameters when utilizing maximum standardized uptake value at the investigated groups

Optimal reconstruction parameters	Iterations number	Subsets number	Optimal postfiltering values (mm)	Matrix size
Group 1	2	18	6	256×256
Group 2	2	24	6	256×256
Group 3	3	18	6.5	256×256
Group 4	3	24	6.5	256×256

Table 5: The recovery coefficients values obtained when utilizing the optimal reconstruction parameters proposed by this study

IEC phantom spheres		RCs	
Diameter (mm)	Volume (mL)	Max	Mean
37	26.52	1.23	1.01
28	11.49	1.21	0.95
22	5.57	1.20	0.91
17	2.57	1.21	0.89
13	1.15	1.03	0.81
10	0.52	0.84	0.61

RCs: Recovery coefficients, IEC: International Electro-technical Commission

Table 6: The optimal selected reconstruction parameters when utilizing maximum standardized uptake value with the routinely used matrix size for investigated groups

Optimal reconstruction parameters	Iterations number	Subsets number	Optimal postfiltering values (mm)	Matrix size
Group 1	2	18	6.5	192×192
Group 2	2	24	6–6.5	192×192
Group 3	3	18	6.5	192×192
Group 4	3	24	6.5	192×192

Table 7: The optimal selected reconstruction parameters when utilizing mean standardized uptake value with the routinely used matrix size for investigated groups

Optimal reconstruction parameters	Iterations number	Subsets number	Optimal postfiltering values (mm)	Matrix size
Group 1	2	18	4	192×192
Group 2	2	24	4	192×192
Group 3	3	18	4	192×192
Group 4	3	24	4	192×192

Discussion

The main purpose of this study was to identify the optimal reconstruction parameters that would produce reliable and consistent RCs, allowing for precise quantification and harmonization for the discovery 710 PET/CT system. As newer generation PET scanners develop, it is necessary to align SUV specifications with the most recent standards and technological advancements.[23,28] The most recent update to the EARL recommendations emphasizes the incorporation of advanced PET technologies, such as TOF and PSF algorithms in PET imaging. These technologies have significantly enhanced spatial resolution and quantitative accuracy in PET imaging. TOF technology uses accurate timing information gained from gamma photon detection, resulting in enhancing localization accuracy. These improvements in accuracy resulted in reducing noise levels and improving contrast in PET imaging. On the

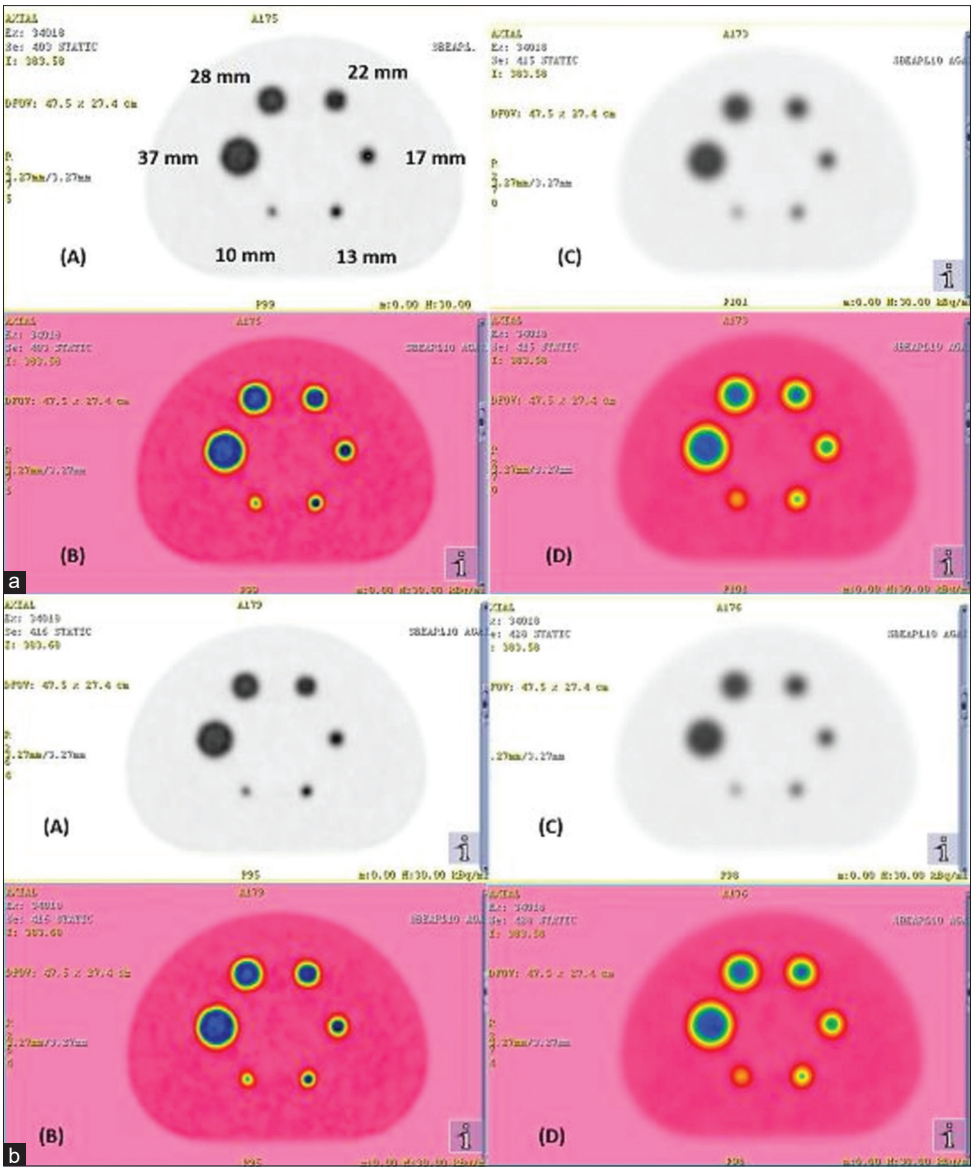

Figure 18: (a) The impact of lowest and highest postfiltering values on SUV qualification and image blurring. It is divided into (A and B) and (C and D) at 4 and 10 mm postfilters, respectively. 2 iteration, 18 subsets and 192 × 192 matrix size were used, (b) The impact of lowest and highest postfiltering values on SUV qualification and image blurring. It is divided into (A and B) and (C and D) at 4 and 10 mm postfilters, respectively. 2 iteration, 18 subset and 256 × 256 matrix size were used

other hand, PSF algorithms account for the blurring effects caused by the detector system and also acting as a filter to minimize noise in reconstructed PET images, hence improving spatial resolution and mitigating PVE.[26,30] In reality, the combined TOF and PSF enable them to complement one another. Previous studies demonstrated that combining TOF and PSF algorithms enhances RCs, particularly for smaller sizes.[7,31] Unfortunately, PSF correction may introduce an upward bias in SUVs values due to the presence of Gibbs artifacts caused by higher voxel-level variance.[17,18] The present work demonstrated that the impact of Gibbs artifacts on RCs quantification is dependent on numerous parameters, including matrix size, number of iterations, number of subsets, and postfiltering value, which is confirmed by.[32] This study demonstrated that SUVmax exhibited higher variability than SUVmean, mostly because SUVmax relies on a single voxel inside a ROI, making it more susceptible to noise, which is consistent with.[5,27,33] Furthermore, several factors can influence the accuracy and reproducibility of SUV measurements. These factors include the size and shape of the lesion being scanned, the PET scanner technology employed, and the selected reconstruction parameters.[27] Newer-generation PET/CT scanners with improved spatial resolution require higher postfiltering values to harmonize SUV measurements. However, increasing the postfiltering values can result in image detectability degradation, particularly for small lesions.[27] The current study found an overestimation/overshooting in RCs values at 13, 17, and 22 mm spheres. This overshooting, known

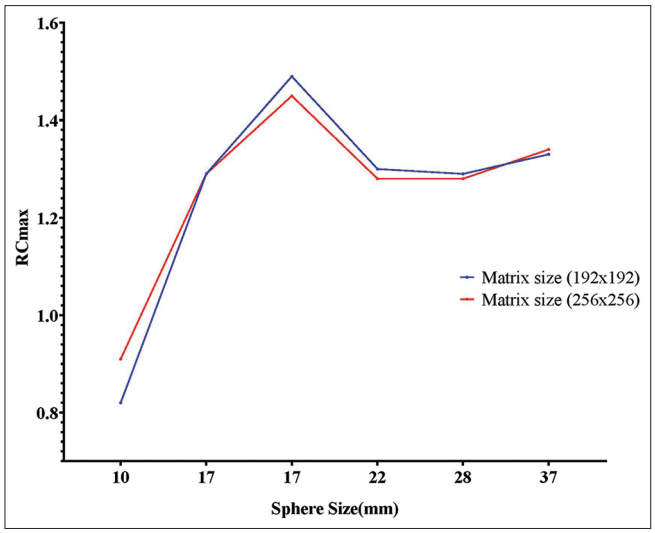

Figure 19: The effect of different matrices sizes on RCma × 2 iterations, 18 subsets, 4 mm postfilter

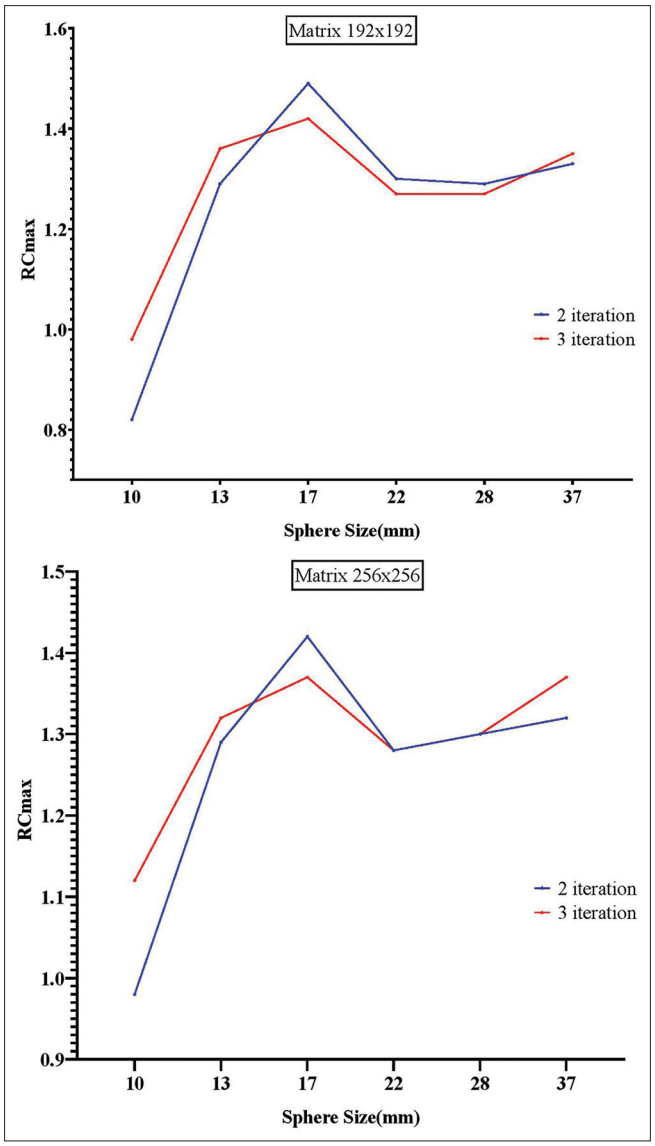

Figure 20: The effect of different iterations numbers on RCmax at different matrices sizes, 18 subsets, 4 mm postfilter

as the Gibbs artifact, resulted in nonmonotonic decreases in RCs, causing unexpected fluctuations rather than a consistent decrease as the sphere sizes decreased, as validated by.[34] Also, Gibbs artifacts affected the RCs of 10, 13 mm spheres, although they compensated for the loss in RCs caused by PVE. These artifacts had a significant effect on the RCmax than the RCmean, which is confirmed by.[27] This study found that increasing postfiltering values can assist mitigate overestimation/overshooting in RCs values for larger spheres. This revealed that higher postfiltering values could lead to more accurate results for larger spheres. However, it should be noted that for smaller-sized spheres, increasing in postfiltering values resulted in a decrease in their RCs and intensified the effect of PVE. Furthermore, the size of the postfilter had a higher impact on image quality and quantification in TOF + PSF images. Utilizing higher postfilter sizes resulted in more significant smoothing and noise reduction, but also increased image blurring. Conversely, reducing the postfilter size decreased image blurring compared to larger voxels, which is consistent with.[19] This study demonstrated that the optimal filter size for SUVmean was 4–4.5 mm, whereas SUVmax was 6–6.5 mm. To address the Gibbs artifact and blurring effect caused by inadequate filtering in reconstructed images, the present study suggests utilizing two sets of reconstructed images. One set should be utilized for spheres detectability purposes and the other for SUV quantification. This approach ensures that appropriate filtering is applied to each set of images, which improves RC quantification while reducing Gibbs artifacts.

When comparing a 256 × 256 matrix to a 192 × 192 matrix, it was observed that larger matrix size had a minimal effect on reducing RC overestimation caused by the Gibbs artifact in larger sphere sizes. Additionally, it slightly decreased the underestimation caused by PVE in smaller sphere sizes. However, the effect of postfiltering on RCs was found to be more significant than the influence of the matrix size. The present study demonstrated that a 256 × 256 matrix size plays a crucial role in minimizing the effects of the Gibbs artifact and PVE across various sphere sizes when appropriate postfiltering is applied, which is consistent with.[35] Furthermore, the optimization of subsets and iterations is crucial for improving computation efficiency and achieving better RCs quantification, as highlighted in existing literature.[25] The present study supports these findings by demonstrating that the number of iterations and subsets significantly influenced the RCs, particularly for small-sized spheres, which is aligned with previous studies.[36,37] Optimizing the number of iterations in the TOF + PSF algorithm resulted in more accurate RCs quantification, which was particularly useful for small-sized spheres where accurate quantification was challenging due to PVE. The underestimation of RCs at small spheres was due to PVE, which increased as the sphere size decreased and decreased as the number of iteration increased. Furthermore, increasing the number of subsets allowed for a

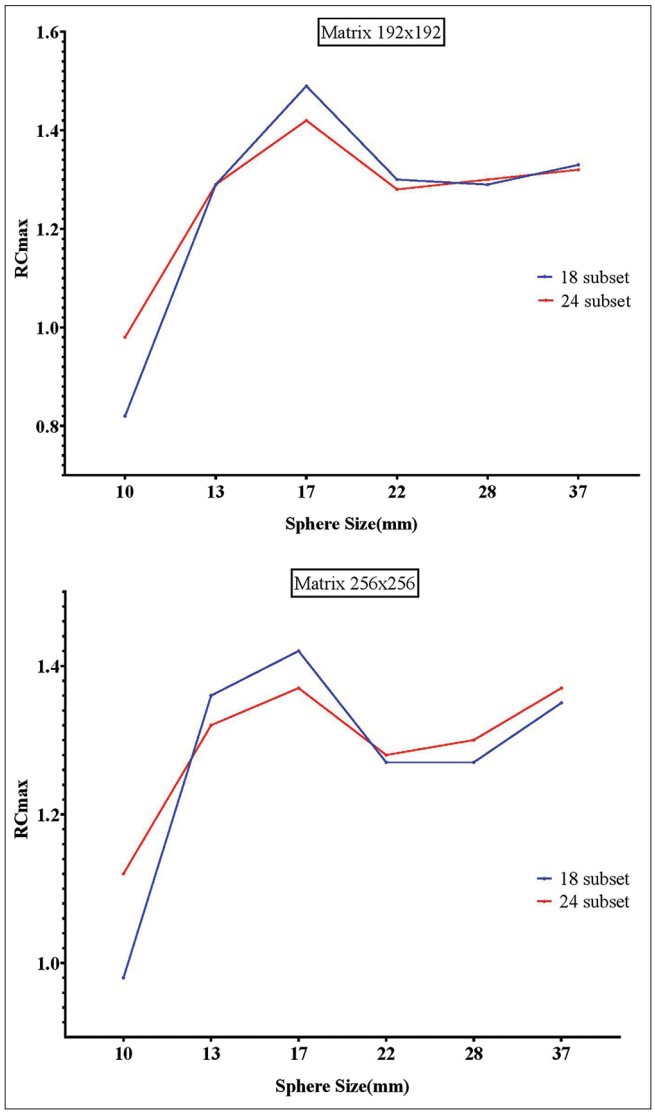

Figure 21: The effect of subset numbers on RCmax at different matrices sizes and 2 iterations and 4 mm post filter

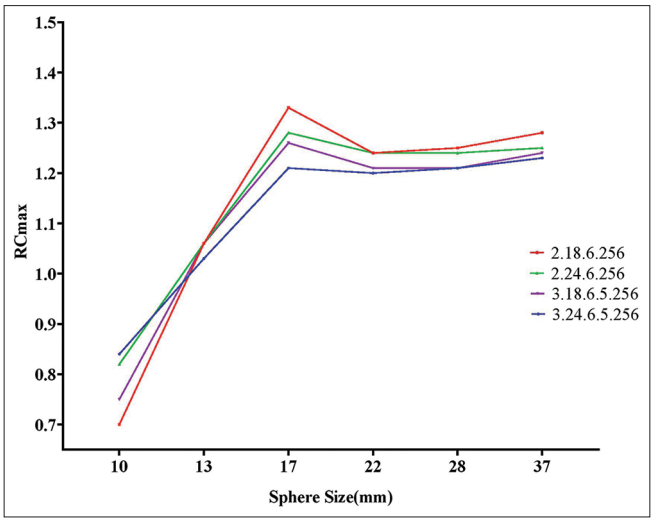

Figure 22: The optimal selected reconstruction parameters for Rcmax at the four investigated reconstruction parameters groups

more comprehensive sampling of the data, which enhanced accuracy in RCs values, especially for small-sized spheres. As a result, this work concluded that combining 3 iterations and 24 subsets optimized the reconstruction process and improved RC quantification at 10 mm sphere.

Visual analysis of RC curves was beneficial to identify abnormal behavior and localized variations, particularly those related to Gibbs artifacts. The selection of the optimized reconstruction parameters was based on the performance of RCmean and RCmax. RCmax tended to exceed unity for sphere sizes ≥13 mm due to the influence of Gibbs artifacts. In contrast, RCmean remained close to or less than unity because it was less affected by Gibbs artifacts. Larger spheres exhibited a higher increase in RCs, resulting in more "flat" RC curves and reducing the dependence of subsequent quantitative analysis on sphere size. For larger spheres ≥17 mm, the RCmax values exceeding unity, indicating an accepted positive bias of approximately 10%–25% for RC, which is confirmed by.[23] Based on our observations, we recommend utilizing a 256 × 256 matrix size with SUVmean to quantify spheres ≥13 mm. SUVmax is best suited for spheres ≤10 mm.

To summarize, the study highlighted the significance of optimizing the reconstruction parameters to achieve accurate quantification of RC. These reconstruction parameters include a matrix size of 256 × 256, a postfiltering value of 6.5 mm, 3 iterations, and 24 subsets, particularly when utilizing SUVmax. The optimal filter size for SUVmean was found to be 4–4.5 mm. These parameters were recognized as effective choices for achieving accurate and reliable SUV quantification in the study's results. These parameters were aligned with the RCs values recommended by the EARL 2 specifications, as presented in Table 5. As a result, adequate reconstruction parameters and careful consideration should be given to the choice of SUV metrics for specific clinical applications.

Conclusion

The study emphasizes the importance of considering a careful choice between SUVmax and SUVmean based on the specific goals of the PET imaging study and the sizes of the spheres being quantified. For quantifying spheres ≥13 mm, SUVmean should be utilized, whereas SUVmax is recommended for spheres ≤10 mm. The selection of appropriate postfiltering values, such as 6–6.5 mm for SUVmax and 4–4.5 mm for SUVmean, significantly improves SUV quantification. Specifically, utilizing 3 iterations, 24 subsets, a postfiltering value of 6.5 mm, and a matrix size of 256 × 256 improved SUVmax quantification. In addition, it is recommended to employ the two sets of reconstructed images, one for diagnosis and the other for SUV quantification.

Limitations

Finally, it is worthnoting that the study was based on a phantom model, which had limitations such as a finite plastic wall thickness, a homogeneous background, and spherical

inserts.[38,39] While phantom studies provide valuable insights and allow for standardized evaluation, caution should be exercised when extrapolating these findings to clinical practice. Nonetheless, such studies can still provide valuable insights into the underlying physics of PET/CT imaging, as well as guidance for optimizing imaging parameters to improve the accuracy and reproducibility of SUV measurements.

Financial support and sponsorship

Nil.

Conflicts of interest

There are no conflicts of interest.

References

1. Boellaard R, Delgado-Bolton R, Oyen WJ, Giammarile F, Tatsch K, Eschner W, *et al.* FDG PET/CT: EANM procedure guidelines for tumour imaging: Version 2.0. Eur J Nucl Med Mol Imaging 2015;42:328-54.
2. Lodge MA. Repeatability of SUV in oncologic (18) F-FDG PET. J Nucl Med 2017;58:523-32.
3. Boellaard R. Standards for PET image acquisition and quantitative data analysis. J Nucl Med 2009;50 Suppl 1:11S-20S.
4. Adams MC, Turkington TG, Wilson JM, Wong TZ. A systematic review of the factors affecting accuracy of SUV measurements. AJR Am J Roentgenol 2010;195:310-20.
5. de Langen AJ, Vincent A, Velasquez LM, van Tinteren H, Boellaard R, Shankar LK, *et al.* Repeatability of 18F-FDG uptake measurements in tumors: A metaanalysis. J Nucl Med 2012;53:701-8.
6. Rausch I, Cal-González J, Dapra D, Gallowitsch HJ, Lind P, Beyer T, *et al.* Performance evaluation of the Biograph mCT Flow PET/CT system according to the NEMA NU2-2012 standard. EJNMMI Phys 2015;2:26.
7. Sunderland JJ, Christian PE. Quantitative PET/CT scanner performance characterization based upon the society of nuclear medicine and molecular imaging clinical trials network oncology clinical simulator phantom. J Nucl Med 2015;56:145-52.
8. Quak E, Le Roux PY, Lasnon C, Robin P, Hofman MS, Bourhis D, *et al.* Does PET SUV harmonization affect PERCIST response classification? J Nucl Med 2016;57:1699-706.
9. Vanderhoek M, Perlman SB, Jeraj R. Impact of different standardized uptake value measures on PET-based quantification of treatment response. J Nucl Med 2013;54:1188-94.
10. Geworski L, Knoop BO, de Cabrejas ML, Knapp WH, Munz DL. Recovery correction for quantitation in emission tomography: A feasibility study. Eur J Nucl Med 2000;27:161-9.
11. Di Martino F, Barca P, Bortoli F, Giuliano A, Volterrani D. Correction for the partial volume effects (PVE) in nuclear medicine imaging: A post-reconstruction analytic method. Appl Sci 2021;11:1-14.
12. Vandenberghe S, Mikhaylova E, D'Hoe E, Mollet P, Karp JS. Recent developments in time-of-flight PET. EJNMMI Phys 2016;3:3.
13. Harrison RL, Alessio AM, Kinahan PE, Lewellen ST. Signal to noise ratio in simulations of time-of-flight positron emission tomography. IEEE Nucl Sci Symp Conf Rec 2004;7:4080-3.
14. Surti S, Karp JS, Popescu LM, Daube-Witherspoon ME, Werner M. Investigation of time-of-flight benefit for fully 3-D PET. IEEE Trans Med Imaging 2006;25:529-38.
15. Cho S, Ahn S, Li Q, Leahy RM. Analytical properties of time-of-flight PET data. Phys Med Biol 2008;53:2809-21.
16. El Fakhri G, Surti S, Trott CM, Scheuermann J, Karp JS. Improvement in lesion detection with whole-body oncologic time-of-flight PET. J Nucl Med 2011;52:347-53.
17. Armstrong IS, Kelly MD, Williams HA, Matthews JC. Impact of point spread function modelling and time of flight on FDG uptake measurements in lung lesions using alternative filtering strategies. EJNMMI Phys 2014;1:99.
18. Tsutsui Y, Awamoto S, Himuro K, Umezu Y, Baba S, Sasaki M. Characteristics of smoothing filters to achieve the guideline recommended positron emission tomography image without harmonization. Asia Ocean J Nucl Med Biol 2018;6:15-23.
19. Shekari M, Ghafarian P, Ahangari S, Ghadiri H, Bakhshayeshkaram M, Ay MR. Optimizing Image Reconstruction Parameters in Time of Flight PET/CT Imaging: a Phantom Study. Frontiers Biomed Technol 2015;2:146-54.
20. EARL. EANM FDG PET/CT accreditation specifications for SUV recovery coefficients. 2017. Available from: http://earl.eanm.org/cms/website.php. [Last accessed 2024 May 01].
21. Lasnon C, Quak E, Le Roux PY, Robin P, Hofman MS, Bourhis D, *et al.* EORTC PET response criteria are more influenced by reconstruction inconsistencies than PERCIST but both benefit from the EARL harmonization program. EJNMMI Phys 2017;4:17.
22. Boellaard R, O'Doherty MJ, Weber WA, Mottaghy FM, Lonsdale MN, Stroobants SG, *et al.* FDG PET and PET/CT: EANM procedure guidelines for tumour PET imaging: Version 1.0. Eur J Nucl Med Mol Imaging 2010;37:181-200.
23. Kaalep A, Sera T, Rijnsdorp S, Yaqub M, Talsma A, Lodge MA, *et al.* Feasibility of state of the art PET/CT systems performance harmonisation. Eur J Nucl Med Mol Imaging 2018;45:1344-61.
24. National Electrical Manufacturers Association. NEMA Standards Publication NU 2-2007: performance measurements of positron emission tomographs;2007.
25. Yoon HJ, Jeong YJ, Son HJ, Kang DY, Hyun KY, Lee MK. Optimization of the spatial resolution for the GE discovery PET/CT 710 by using NEMA NU 2-2007 standards. J Korean Phys Soc 2015;66:287-94.
26. Vennart NJ, Bird N, Buscombe J, Cheow HK, Nowosinska E, Heard S. Optimization of PET/CT image quality using the GE 'Sharp IR' point-spread function reconstruction algorithm. Nucl Med Commun 2017;38:471-9.
27. Monsef A, Ay MR, Sheikhzadeh P, Geramifar P, Rahmim A, Ghafarian P. Harmonization based on quantitative analysis of standardized uptake value variations across PET/CT scanners: A multicenter phantom study. Nucl Med Commun 2022;43:1004-14.
28. EANM/EARL. Accreditation specifications – EANM EARL – Research4Life. Available from: https://earl.eanm.org/accreditation-specifications/. [Last accessed on 2023 Feb 14].
29. Morey AM, Noo F, Kadrmas DJ. Effect of using 2mm voxels on observer performance for PET lesion detection. IEEE Trans Nucl Sci 2016;63:1359-66.
30. Salvadori J, Odille F, Verger A, Olivier P, Karcher G, Marie PY, *et al.* Head-to-head comparison between digital and analog PET of human and phantom images when optimized for maximizing the signal-to-noise ratio from small lesions. EJNMMI Phys 2020;7:11.
31. Kaalep A, Sera T, Oyen W, Krause BJ, Chiti A, Liu Y, *et al.* EANM/EARL FDG-PET/CT accreditation – Summary results from the first 200 accredited imaging systems. Eur J Nucl Med Mol Imaging 2018;45:412-22.
32. Tsutsui Y, Awamoto S, Himuro K, Umezu Y, Baba S, Sasaki M. Edge artifacts in point spread function-based PET reconstruction in relation to object size and reconstruction parameters. Asia Ocean J Nucl Med Biol 2017;5:134-43.
33. Burger IA, Huser DM, Burger C, von Schulthess GK, Buck A. Repeatability of FDG quantification in tumor imaging: Averaged SUVs are superior to SUVmax. Nucl Med Biol 2012;39:666-70.
34. Munk OL, Tolbod LP, Hansen SB, Bogsrud TV. Point-spread function reconstructed PET images of sub-centimeter lesions are not quantitative. EJNMMI Phys 2017;4:5.
35. Ptáček J, Karhan P, Fiala P. Optimal reconstruction matrix and PET image filtration for point-spread function and time-of-flight reconstruction – A phantom study. Phys Med 2017;39:95-9.
36. Ashrafinia S, Mohy-Ud-Din H, Karakatsanis NA, Jha AK, Casey ME, Kadrmas DJ, *et al.* Generalized PSF modeling for optimized quantitation in PET imaging. Phys Med Biol 2017;62:5149-79.
37. Morey AM, Kadrmas DJ. Effect of varying number of OSEM subsets on PET lesion detectability. J Nucl Med Technol 2013;41:268-73.
38. Hofheinz F, Dittrich S, Pötzsch C, Hoff JV. Effects of cold sphere walls in PET phantom measurements on the volume reproducing threshold. Phys Med Biol 2010;55:1099-113.
39. Berthon B, Marshall C, Edwards A, Evans M, Spezi E. Influence of cold walls on PET image quantification and volume segmentation: A phantom study. Med Phys 2013;40:(082505-1)-(082505-13).